

Diverse Sample Generation: Pushing the Limit of Data-free Quantization

Haotong Qin, Yifu Ding, Xiangguo Zhang, Aoyu Li, Jiakai Wang, Xianglong Liu*, Jiwen Lu

Abstract—Recently, generative data-free quantization emerges as a practical approach that compresses the neural network to low bit-width without access to real data. It generates data to quantize the network by utilizing the batch normalization (BN) statistics of its full-precision counterpart. However, our study shows that in practice, the synthetic data completely constrained by BN statistics suffers severe homogenization at distribution and sample level, which causes serious accuracy degradation of the quantized network. This paper presents a generic **Diverse Sample Generation (DSG)** scheme for the generative data-free post-training quantization and quantization-aware training, to mitigate the detrimental homogenization. In our DSG, we first slack the statistics alignment for features in the BN layer to relax the distribution constraint. Then we strengthen the loss impact of the specific BN layer for different samples and inhibit the correlation among samples in the generation process, to diversify samples from the statistical and spatial perspective, respectively. Extensive experiments show that for large-scale image classification tasks, our DSG can consistently outperform existing data-free quantization methods on various neural architectures, especially under ultra-low bit-width (e.g., 22% gain under W4A4 setting). Moreover, data diversifying caused by our DSG brings a general gain in various quantization methods, demonstrating diversity is an important property of high-quality synthetic data for data-free quantization.

Index Terms—data-free quantization, quantized neural networks, data generation, model compression, deep learning.

arXiv:2109.00212v2 [cs.CV] 3 Sep 2021

1 INTRODUCTION

With the advent of deep learning, the deep convolutional neural network has achieved a great success in a variety of fields, such as image classification [25], [45], [47], [51], [52], [56], [57], object detection [16], [17], [29], [37], [42], [55], semantic segmentation [13], [62], etc. Nevertheless, it is still a significant challenge to apply advanced neural networks on resource-limited devices for its high memory usage and expensive computation. With more and more hardware supporting low bit-width computations [4], [11], [31], [40], [41], [49], [50], [53], [54], [63], network quantization emerges as an efficient method to compress and accelerate models. Many quantization methods, called the quantization-aware training (QAT), apply the following pipeline: considering the quantization function in the whole finetuning (retaining) process on the original dataset, and minimizing the loss caused by the quantization through backward propagation. Since QAT methods require the finetuning steps, it is considered to be time-consuming and computationally intensive [18], [24], [39]. Thus, quantization without training or finetuning process is also demanded in the industry, which is called post-training quantization (PTQ) in recent studies [2], [9], [30], [34], [61].

Most existing quantization methods are data-driven that require real data in their quantization process. However, for privacy or security concerns, real data is not always accessible (e.g., medical and user data). Fortunately, data-free quantization is proposed to quantize the network without access to real data. And as shown in

Haotong Qin is with the State Key Laboratory of Software Development Environment and Shen Yuan Honors College, Beihang University; Yifu Ding, Xiangguo Zhang, Aoyu Li, Jiakai Wang, and Xianglong Liu are with the State Key Laboratory of Software Development Environment, Beihang University (Corresponding author: Xianglong Liu); Jiwen Lu are with the Department of Automation, Tsinghua University. Email: {qinhaotong,zjdyf,xianguozhang,jk_buaa_scse,xlliu}@buaa.edu.cn, lujiwen@tsinghua.edu.cn. Our code is released at <https://github.com/htqin/DSG>.

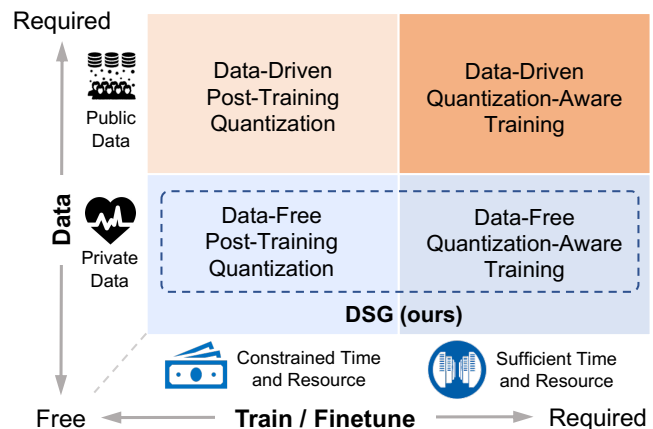


Fig. 1: The existing quantization approaches can be quartered by data-required or not and train/finetune-required or not. Our diverse sample generation method is proposed for data-free quantization methods including data-free post-training quantization (PTQ) and quantization-aware training (QAT)

Fig. 1, the data-free quantization approaches can also be classified as data-free PTQ and QAT according to whether the network training/finetuning is required. The data-free PTQ obtains the quantized network through computation-saving calibration [5], [35], [59], while the data-free QAT finetune the whole quantized network to let it be more accurate [8], [23], [32], [44]. Most of the existing data-free quantization methods (ZeroQ [5] and GDFQ [44] as the representative) generate the "optimal synthetic data" with the distribution that best matches the Batch Normalization (BN) statistics of the original full-precision neural network. Since the synthetic data is used to calibrate or finetune to the quantized network in these methods, they are called generative data-free quantization methods as usual. Among these methods, the data-

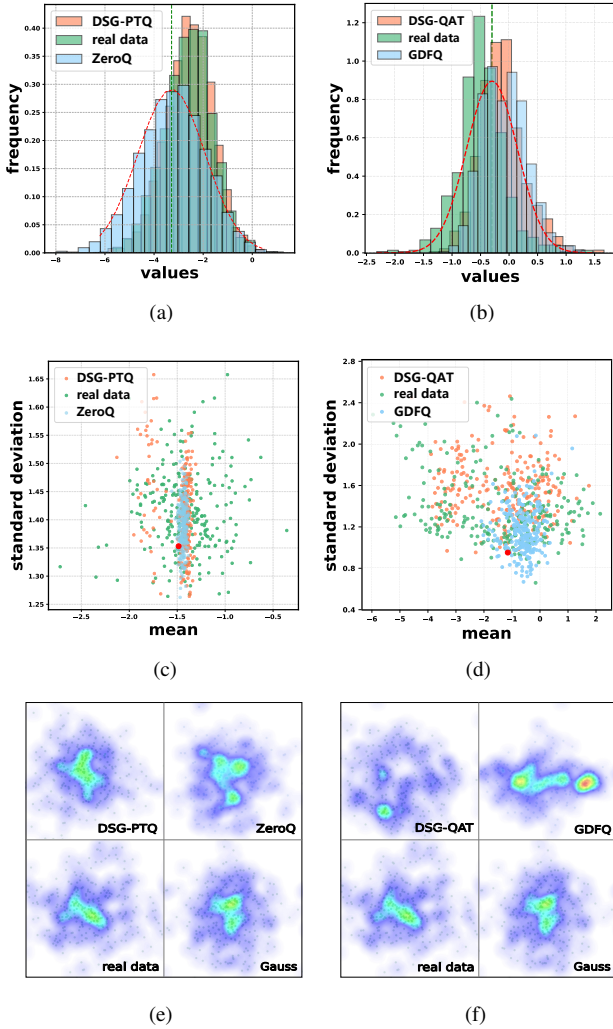


Fig. 2: Comparison between real data (random sampling from ImageNet) and data synthesized by generative data-free quantization methods (DSG and ZeroQ for PTQ in the first column, DSG and GDFQ for QAT in the second column) with 256 samples of each. (a) and (b) show the activation distribution of one channel in ResNet18 for PTQ and QAT, respectively. (c) and (d) are charts of the mean and standard deviation for one channel of synthetic data. (e) and (f) are the visualization of the synthetic data after dimensionality reduction in the sample space

free PTQ methods apply BN statistics loss to directly update the generated data without considering the calibration process [5], [59]; while the QAT methods usually introduce a separate generator for better synthetic data since the sufficient resources and time, and train the generator and the quantized network jointly [8], [23], [32], [44].

However, for existing quantization methods, the networks quantized with the real data always outperform those quantized with synthetic data of existing data-free quantization methods. Our study reveals that severe homogenization problems prevent the quantized neural network from satisfactory performance, which exists in the data generation process in typical data-free generative quantization methods. First, the synthetic data is constrained to match the BN statistics, and thereby the feature distribution might overfit the BN statistics in each layer when the data forward propagate in models. As shown in Fig. 2(a) and Fig. 2(b), the distribution of samples synthesized by generative data-free PTQ and QAT methods

(ZeroQ and GDFQ) almost strictly follow the Gaussian distribution with corresponding BN mean and variance, while the distribution of real data has an obvious offset and enjoys a more diverse distribution. We consider this phenomenon as the **distribution-level homogenization**. Second, all samples of synthetic data are updated by one specific objective function in typical generative data-free quantization methods. Taking ZeroQ and GDFQ as examples, both of them use the same constraint for all synthetic samples that directly sum the loss term of each layer. In Fig. 2(c) and Fig. 2(d), the distribution statistics of real data are dispersed while the data generated by existing approaches are centralized. Moreover, for data-free QAT methods, synthetic samples are synthesized by a generator network. In the process of learning the distributions of synthetic data for quantization, both the generator and the quantized network may converge to a trivial solution where the former learns to produce few modes exclusively, which is referred to by mode collapse and causes the synthetic data to clustered in sample space [12]. The Fig. 2(e) and Fig. 2(f) are the visualization of the synthetic data after dimensionality reduction with Principal Component Analysis (PCA) [14] in the sample space. The synthetic data of GDFQ are aggregated, while the real data and synthetic data in PTQ are scattered. These phenomena are considered to be **sample-level homogenization** from the statistical and spatial perspectives. In a word, the distribution-level homogenization means that the overall distribution of synthetic data is strictly restricted to the specific distribution (Gaussian distribution with BN statistics), while the sample-level homogenization means the little differences among samples from the statistical and spatial perspectives. Therefore, only mitigating homogenization at one certain level cannot ensure the diversity of data at the other level.

To alleviate the degeneration of the quantized network caused by the homogenization of synthetic data, this paper presents an efficient data generation scheme, **Diverse Sample Generation (DSG)**, for generative data-free quantization to enhance the diversity of the synthetic data. The proposed DSG scheme mainly relies on three novel techniques: *Slack Distribution Alignment (SDA)*: relax the distribution constraint by slacking the feature statistics alignment in each BN layer. *Layerwise Sample Enhancement (LSE)*: strengthen the impact of statistics loss of the specific BN layer for its corresponding synthetic samples by applying a layerwise enhancement. *Sample Correlation inhibition (SCI)*: weaken the correlation among the synthetic samples by applying determinantal point processes loss to the intermediate features in the generation process. Among these techniques, SDA diversifies the synthetic data at the distribution level, while LSE and SCI diversify it at the sample level from the statistical and spatial perspective, respectively. In our DSG, the proposed techniques can be applied to different quantization scenarios effectively, including PTQ and QAT, to improve the performance of the quantized network by diversifying synthetic data.

Our scheme presents a novel perspective of data diversity for generative data-free quantization, and extensive experiments show that DSG significantly improves both data-free PTQ and QAT. The DSG performs remarkably well across several mainstream neural architectures, including VGG16bn [45] (the VGG16 with BN for the dense layers), ResNet20/18/50 [21], SqueezeNext [15], InceptionV3 [48], ShuffleNet [60], and MobileNetV2 [43], and surpasses the existing data-free methods in a wide margin on the large-scale image classification task and achieves the state-of-the-art (SOTA) results. The quantized networks quantized by our DSG even outperform networks quantized by the real data under the

various setting. The performance of the low bit-width networks trained by our DSG scheme is close to that of full-precision counterparts. Meanwhile, it gets rid of the data dependence in the quantization process.

We summarize the main contributions of this paper as:

- 1) We propose a novel generic DSG scheme for generative data-free quantization from a comprehensive perspective of data diversity, which effectively improves the data-free PTQ and QAT.
- 2) We further study the data homogenization problems of synthetic data in generative data-free quantization. The study presents the homogenization at the distribution and sample level and further reveals that the sample-level homogenization is not limited to the statistical perspective, but also the spatial perspective. Thus, we present a novel Sample Correlation Inhibition (SCI), in conjunction with the Slack Distribution Alignment (SDA) and Layerwise Sample Enhancement (LSE) techniques to diversify synthetic data at distribution and sample level.
- 3) We conduct a detailed ablation study on the proposed DSG and evaluate the scheme on various neural architectures. The results show the improvements of the proposed techniques (SDA, LSE, and SCI) in generative data-free PTQ and QAT, and that our DSG surpasses the existing SOTA methods by a wide margin.
- 4) We also conduct more studies on synthetic data of generative data-free quantization methods. Benefits from the enhanced diversity, the performance of quantized networks in various methods (calibration and data-driven quantization methods) integrating with DSG data are significantly improved, which presents that diversity is an important property of high-quality synthetic data.

Note that our paper extends the preliminary conference paper [59]. Our paper proposed a novel generic DSG scheme for generative data-free PTQ and QAT, while the method proposed in the conference paper can be regarded as a special case in PTQ. And we make further exploration and reveal the sample-level homogenization from the spatial perspective in data-free QAT and present a novel SCI to tackle the problem, which significantly improves the performance of generative data-free QAT. We evaluate our DSG scheme on various neural architectures and compared it with more data-free PTQ and QAT methods. Besides, we further add more analysis and discussion of synthetic data and evaluate the data with various methods. The results present that diversity is an important property of high-quality synthetic data in generative data-free quantization.

2 RELATED WORK

Data-driven Quantization. As a widely used compression technique, quantization earns lots of attention in recent years. To mitigate the severe accuracy drop resulted from quantization, many studies, such as [18], [24], [54], [63], utilize quantization-aware training methods to regain the accuracy. Generally, they can always provide performance improvements. However, the training process is quite cumbersome for huge computational and time costs. Another critical deficiency is that the datasets are not always ready to use, especially for privacy and security concerns. Without any finetuning or training process, research of post-training quantization has been conducted to improve the trade-off between accuracy and computational cost. [2] introduces two closed-form analytical solutions targeting clipping approximation and per-channel bit allocation combined with bias-correction to push the limit of weights and activations quantization to 4-bit. [9] analyzes the mean squared error of quantization and minimizing it via the OMSE

method. Unlike previous work which aims to find an appropriate clipping range to deal with outliers in the bell-shaped distribution, [61] proposes outlier channel splitting while remains a functionally identical network. Not restricted to the round-to-nearest method, [34] exploits a more flexible weight-rounding mechanism called AdaRound, which optimizes task loss due to quantization w.r.t. the preactivation. However, these methods still require access to the limited data for a more resilient and better-quantized model.

Data-free Quantization. Several recent studies have explored quantization methods without training and even calibration datasets. [35] uses weight equalization to acquire similar weight ranges among channels and bias correction for activations. However, quantizing models to run in 6-bit or lower bit-width is a non-trivial task. Works like [19], [5] and [23] leverage BN statistics to reconstruct "realistic" data. Both [19] and [44] utilizes knowledge distillation scheme to finetune the model, while it might cost a little more time. [19] proposes an inception scheme to generate data, while [23] utilizes a generative modeling to deal with the distribution of BN statistics. Besides, [5] can work on multi-bit quantization utilizing the Pareto frontier. [8] and [32] focuses on adversarial approaches. [8] proposes a data-free adversarial knowledge distillation method, which minimizes the maximum distance between the outputs of the full-precision teacher model and the quantized student model for any adversarial samples from a generator. [32] instead not only considers the output of model layer but also maximizes the discrepancy of feature map in intermediate inter-channel between teacher and student model by the proposed Channel Relation Map. Although the above methods use distinct tricks to synthesize data and improve model accuracy, they all have similar limitations and we take [5] as an example to illustrate in Section 3.2 specifically.

3 METHODS

In this section, we first revisit previous works about data generation in data-free quantization. Then, we reveal the homogenization phenomenon, and make efforts on improving the generation process to diversify the samples of synthetic data.

3.1 Preliminaries

Existing data-driven quantization methods require original training and testing datasets to calibrate or finetune the quantized network for higher performance. But the real data is not accessible in many practical applications for privacy or security concerns, and thereby general quantization schemes cannot be applied directly to these scenarios. The data-free quantization is proposed to quantize the network without access to real data.

3.1.1 Generative Data-free Quantization

Given a neural network M , generative data-free quantization aims to generate synthetic data x^s and meanwhile quantize the network to low-bit. As mentioned in Section 1, data-free PTQ and QAT are applied in scenarios where resources and time are limited and sufficient, respectively. Therefore, the generative data-free PTQ directly updates the data from random vectors during the generation process, and then uses the synthetic data to calibrate (rather than finetune) the quantized network; while the generative data-free QAT trains a separate generator network to synthesize the data and uses them to finetune the quantized network.

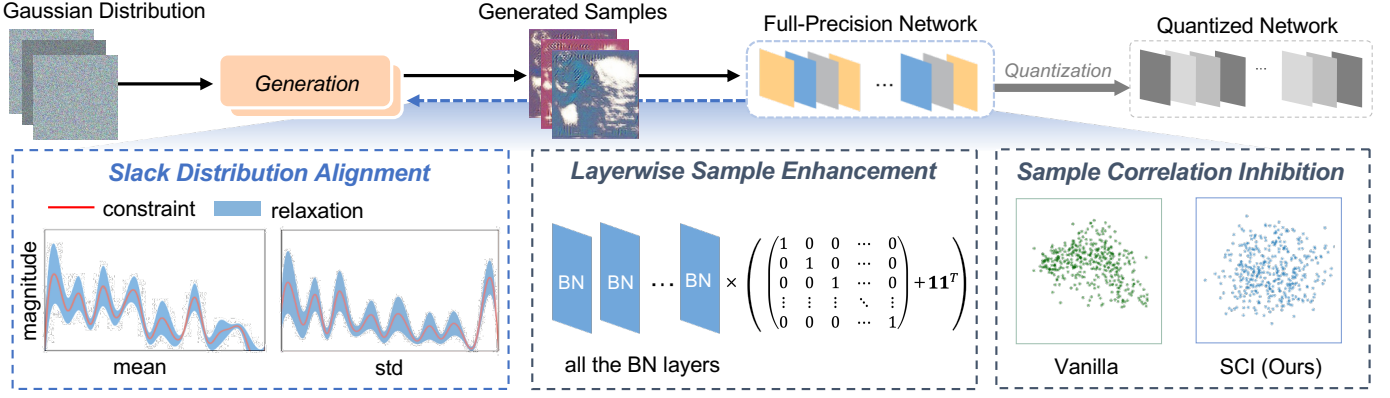


Fig. 3: The overview of the Diverse Sample Generation (DSG) scheme for data-free quantization. The proposed three techniques are applied to the generation process: Slack Distribution Alignment (SDA) relaxes BN statistics constraint in each layer; Layerwise Sample Enhancement (LSE) provides a specific loss term for each sample; Sample Correlation Inhibition (SCI) diversifies the synthetic data in sample space. The first one diversifies synthetic data at the distribution level, and the latter two at the sample level

For generative data-free PTQ, the optimization objective can be expressed as

$$\min_{\mathbf{x}^s} \mathcal{L}_{\text{PTQ}}(\mathbf{x}^s, \mathbf{M}), \quad (1)$$

and \mathbf{x}^s is optimized directly by reducing the loss function $\mathcal{L}(\cdot, \cdot)$ (typically KL divergence and BN statistics loss). While for the tolerance of computational complexity in generative data-free QAT, we usually use an extra generator network G to synthetic data. Formally, we define the generation process as follows:

$$\mathbf{x}^s = G(\mathbf{z}), \quad \mathbf{z} \sim \mathcal{N}(0, 1), \quad (2)$$

where \mathbf{z} is a random tensor drawn from standard Gaussian distribution $\mathcal{N}(0, 1)$, \mathbf{x}^s and y are synthetic data and the corresponding label. In this case, the quantized network Q and synthetic data (\mathbf{x}^s, y) are optimized simultaneously:

$$\min_G \mathcal{L}_{\text{QAT}}(G(\mathbf{z}), \mathbf{M}), \quad \min_Q \mathbb{E}_{\mathbf{x}^s, y} [\mathcal{C}(Q(\mathbf{x}^s), y)], \quad (3)$$

where $\mathcal{C}(\cdot, \cdot)$ is a loss function for quantized network Q , such as cross-entropy loss and mean squared error.

3.1.2 BN Statistics Loss for Generation

As mentioned above, the knowledge about the real data in the pre-trained network should be fully exploited. The \mathcal{L}_{PTQ} and \mathcal{L}_{QAT} in Eq. (1) and Eq. (3) aims to constrain and update the synthetic data (or generator) through exploiting the knowledge in the full-precision network \mathbf{M} , and then use the data to calibrate or finetune the quantized network. Since the statistics (mean and standard deviation) of BN layer fit the original real dataset in the training process, most data-free quantization schemes utilize the information in the BN statistics to construct synthetic data.

The following optimization objective enables the distribution of synthetic data \mathbf{x}^s to best match the BN statistics, including the mean and standard deviation:

$$\min_{\mathbf{x}^s} \mathcal{L}_{\text{BN}} = \sum_{i=0}^N \|\tilde{\boldsymbol{\mu}}_i^s - \boldsymbol{\mu}_i\|_2^2 + \|\tilde{\boldsymbol{\sigma}}_i^s - \boldsymbol{\sigma}_i\|_2^2, \quad (4)$$

where $\tilde{\boldsymbol{\mu}}_i^s$ and $\tilde{\boldsymbol{\sigma}}_i^s$ are the mean and standard deviation of feature distribution of synthetic data \mathbf{x}^s at i -th BN layer, while $\boldsymbol{\mu}_i$ and $\boldsymbol{\sigma}_i$ are that of pre-trained full-precision model \mathbf{M} . By minimizing the BN statistics loss \mathcal{L}_{BN} , network learns a distribution of input data to best match BN statistics of each layer.

3.2 Homogenization of Synthetic Data

The generative data-free quantization well sidesteps the issue of lacking accessibility of real data, but we have to concede the huge performance drop compared with networks quantized with real data. From the existing image synthesizing methods in data-free quantization, we discover the homogenization phenomena, which degrade the fidelity and quality of synthetic data. We conclude the homogenization of synthetic data into distribution level and sample level to elaborate on them.

3.2.1 Distribution-level Homogenization

Since the performance of existing data-driven quantization significantly surpasses that of data-free quantization in usual, the original training data (real data) is generally considered as the upper limit of the performance of synthetic data. So as Eq. (4) shows, methods constrained by \mathcal{L}_{BN} are dedicated to generating samples by confining the feature statistics of synthetic data around BN statistics of the pre-trained model. However, the data from the real world is always more diverse, while that generated by fitting BN statistics suffers constrained features as shown in Fig. 2(a) and Fig. 2(b). The activation distribution of data generated in ZeroQ and GDFQ (the SOTA generative data-free PTQ and QAT methods) well fit the normal distribution of BN statistics while that of real data deviates from BN statistics. When we calculate the Wasserstein distance between the Gaussian distribution with BN statistics and the feature distribution of synthetic data, the index values of the existing methods are significantly smaller than the real data (real data 0.120 vs ZeroQ 0.040 in PTQ, and real data 0.134 vs GDFQ 0.116 in QAT). We consider it as distribution-level homogenization causing by the strict constraint applied to the synthesizing process makes the synthetic data overfit BN statistics in each layer.

3.2.2 Sample-level Homogenization

Besides homogenization at the distribution level, synthetic data in existing generative data-free quantization also suffer the homogenization at the sample level.

1) From the statistical perspective: in existing generative data-free methods, such as ZeroQ and GDFQ, all samples are constrained by the identical form of BN statistics loss. So there might be little difference among statistics of synthetic samples in one batch, while samples from the real world are diverse. As shown in Fig. 2(c) and Fig. 2(d), the points of the mean and standard

deviation of ZeroQ and GDFQ data are significantly overlapping and all points gather together closely near BN statistics. However, statistics of real data and our DSG data have larger variance and are more dispersed. Taking PTQ as an example, the variance of the statistics of the real sample is 0.029, that much larger than the variance of data generated by ZeroQ, which is 0.009.

2) From the spatial perspective: the synthetic samples generated in different ways have different behaviors. For existing data-free QAT methods, all samples are synthesized by the same generator. The samples generated by GDFQ are concentrated in spatial perspective, as shown in Fig. 2(f), while samples of our DSG and real data are more scattered. The heatmap shows the degree of aggregation in the synthetic data sample space. The densest cluster of GDFQ samples appears red in the heatmap and the density index is up to 2052 near the cluster center, while the highest density index of the real sample is only 1681.

However, for PTQ methods, there are no significant differences among the four types of samples as shown in Fig. 2(e). It seems that the sample-level homogenization from the spatial perspective is a particular property in data-free generative QAT methods. We regard these as sample-level homogenization from the statistical and spatial perspectives, which leads to a significant performance drop for the networks quantized by synthetic data.

In a nutshell, for the generation process in data-free quantization, homogenization exists in two levels, i.e. distribution level, and sample level. Thus models quantized with these data can hardly achieve high performance. In this paper, we make efforts to make synthetic data more diverse. We propose a novel data-free quantization scheme to tackle the homogenization issue and further enhance the diversity of synthetic data, which we call the Diverse Sample Generation (DSG) scheme. Data generated by our scheme enables the quantized network to achieve better performance.

3.3 Diverse Sample Generation

We present a generic Diverse Sample Generation (DSG) scheme for both generative data-free PTQ and QAT (Fig. 3). In what follows, we introduce three novel techniques to alleviate homogenization from two aspects. Slack Distribution Alignment in Section 3.3.1 is designed to relaxing the statistical constraint and mitigate distribution-level homogenization, while Layerwise Sample Enhancement in Section 3.3.2 and Sample Correlation Inhibition in Section 3.3.3 are motivated by improving the generation process and further diversify the synthetic data at the sample level.

3.3.1 Slack Distribution Alignment

To deal with distribution-level homogenization, we propose Slack Distribution Alignment (SDA). Specifically, we add relaxation constants during the process of matching original BN statistics, which can be intuitively regarded as margins for means and standard deviation. With the relaxation constants, the synthetic samples do not need to fit the BN statistics strictly, and thus can be more diverse in distribution. The loss term of SDA is $\mathbf{l}_{\text{SDA}} = [l_{\text{SDA}_1}, l_{\text{SDA}_2}, \dots, l_{\text{SDA}_N}]^T$, where N is the number of BN layers in the quantized network, and the l_{SDA_i} for i -th BN layer is expressed as follow:

$$l_{\text{SDA}_i} = \|\max(|\tilde{\boldsymbol{\mu}}_i^s - \boldsymbol{\mu}_i| - \delta_i, 0)\|_2^2 + \|\max(|\tilde{\boldsymbol{\sigma}}_i^s - \boldsymbol{\sigma}_i| - \gamma_i, 0)\|_2^2, \quad (5)$$

where δ_i and γ_i denote the relaxation constants for the mean and standard deviation statistics of features at the i -th BN layers.

After introducing toleration between statistics of synthetic data and BN layers, the mean and standard deviation of generated samples fluctuate within a certain range. With relaxed constraints, samples are more diverse and the feature distribution behaves closer to real data.

As we have discussed that real data can be seen as an ideal dataset to calibrate the quantized network, and experimental evidence shows that features of real data also have gaps compared with BN statistics. Thus, we attempt to approximate the gap between the statistics of real data and BN statistics of the original model as a reference to determine the value of δ_i and γ_i . Under real-world scenarios, when the number of samples reaches a huge amount, the components and features of inputs can be approximate to Gaussian assumption. Based on the central limit theorem, we suppose the whole input set is generally consistent with a Gaussian distribution. Thus we set the initial value of δ_i and γ_i by a batch of samples that randomly initialized from Gaussian distribution: **First**, we input 1024 samples initialized by Gaussian distribution with $\mu = 0$ and $\sigma = 1$ into the full-precision network and then save the feature statistics at each BN layer, including the mean and standard deviation of the feature distribution. **Second**, we measure the margin between saved statistics and the corresponding BN statistics, then take percentiles of the margin to initialize δ_i and γ_i :

$$\delta_i = |\tilde{\boldsymbol{\mu}}_i^0 - \boldsymbol{\mu}_i|_\epsilon, \quad \gamma_i = |\tilde{\boldsymbol{\sigma}}_i^0 - \boldsymbol{\sigma}_i|_\epsilon, \quad (6)$$

where $\epsilon \in (0, 1]$ is a hyper-parameter determining the degree of relaxation, and $\tilde{\boldsymbol{\mu}}_i^0/\tilde{\boldsymbol{\sigma}}_i^0$ are mean/standard deviation of the feature of Gaussian initialized data \mathbf{x}^0 at the i -th BN layer. $|\tilde{\boldsymbol{\mu}}_i^0 - \boldsymbol{\mu}_i|_\epsilon$ and $|\tilde{\boldsymbol{\sigma}}_i^0 - \boldsymbol{\sigma}_i|_\epsilon$ denote the ϵ percentile of $|\tilde{\boldsymbol{\mu}}_i^0 - \boldsymbol{\mu}_i|$ and $|\tilde{\boldsymbol{\sigma}}_i^0 - \boldsymbol{\sigma}_i|$, respectively. Intuitively, the larger the value of ϵ , the more relaxing the constraints are in Eq. (5). We empirically set the default value of ϵ as 0.9 to deal with outliers.

3.3.2 Layerwise Sample Enhancement

For the generation processes in existing generative data-free quantization, samples are always generated by the same initialization and optimization strategy. Specifically, each sample shares the same objective function which directly sums the loss of each layer. That is to say, all the layers receive just as much attention from each sample, and thus results in the homogenization among samples. We propose Layerwise Sample Enhancement (LSE) to tackle sample-level homogenization. Concretely, to enable each sample to focus on statistics of different layers, we build connections between a specific layer and each sample by enhancing its loss term in backward propagation. In other words, we provide various loss functions for each sample. So that, samples in one batch could be different.

Given a network containing the N number of BN layers, earlier works treat each layer the same way without particular predilection or bias. But in LSE, we engineer N different loss terms and apply each of them to the specific data sample. Here, we suppose to generate N samples in one batch, equaling to the number of BN layers of the quantized network. The loss term of LSE for the i -th sample is as follow:

$$l_{\text{LSE}_i} = (\mathbf{1} + \mathbf{h}_i)^T \mathbf{l}, \quad (7)$$

where $\mathbf{1}$ denotes a column vector of all ones, \mathbf{h}_i is an N -dim one-hot column vector where the 1 is in the i -th position, $\mathbf{l} = [l_0, l_1, \dots, l_N]^T$ is the vector of the original loss terms for all BN layers. The set of loss functions for all samples can be expressed

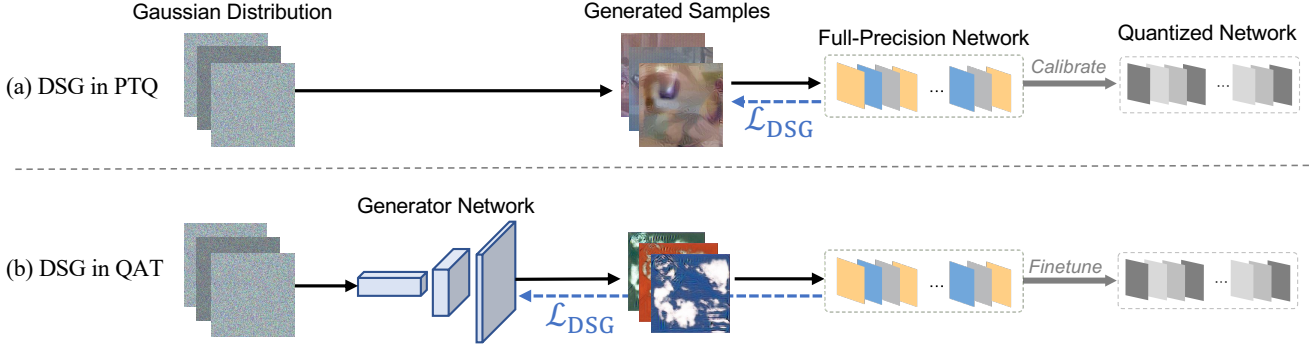


Fig. 4: The procedures of our DSG for specific quantization scenarios. The case (a) is the DSG in PTQ and the case (b) is in QAT

as $\mathbf{X}_{LSE}\mathbf{l} = [l_{LSE_1}, l_{LSE_2}, \dots, l_{LSE_N}]^T$, which is an N -dim column vector and its i -th element represents the loss function for i -th sample in the batch. Thus, for the whole set of samples \mathbf{x}^s , the effect exerted by LSE can be formulated as

$$\mathbf{X}_{LSE} = \mathbf{1}\mathbf{1}^T + [\mathbf{h}_1, \mathbf{h}_2, \dots, \mathbf{h}_N], \quad (8)$$

where \mathbf{X}_{LSE} can be seen as the enhancement matrix for loss terms. In this way, we focus on every BN layer of the original model respectively and generate corresponding samples for each layer. By such layerwise enhancement, we optimize the whole batch of synthetic samples simultaneously.

3.3.3 Sample Correlation Inhibition

In addition to improving the loss function constraining the statistics of synthetic data, we construct the unsupervised Sample Correlation Inhibition (SCI) loss for the samples to diversify the synthetic data from the spatial perspective. We drew inspiration from the determinant point process, and inhibit the correlation among these sample items by dispersing their intermediate features in the generation process, and thereby the sample-level homogenization is alleviated from the spatial perspective.

The determinant point process \mathcal{P} can express negative interactions among samples by the similarity kernel \mathbf{K}_S of the elements in a set \mathbf{S} , where a large value of $\mathbf{K}_{ij}; i, j \in \mathbf{S}$ reduces the likelihood of both elements to appear together in a diverse subset [3], [27]. And it is widely used to generate or select the diverse samples in many existing works, e.g., constraining the synthetic samples in the generative adversarial network for its diversity closer to the real data [6], [12]. However, real data is inaccessible in generative data-free quantization, and thereby it cannot be used to construct the constraint of the diversity of synthetic data. Therefore, we utilize random samples in our SCI instead of the real data, and the random data is applied as a lower bound of diversity to alleviate the homogenization of synthetic samples. Gaussian sampling is used to initialize the synthetic data, so the sampled data can be considered to suffer less homogenization due to the complete independence and random sampling process. In this way, the homogenization of synthetic data is limited to a level lower than its initial state, i.e., it will not bring additional homogenization in the generation process.

We present our SCI in detail below. The intermediate features correspond to the data \mathbf{x}^s in the generation process is expressed as $\mathbf{f} = \{f_1, f_2, \dots, f_N\}$, where f_i is the feature of corresponding synthetic sample. And for the set of features \mathbf{f} , we construct a set of random vectors $\mathbf{r} = \{r_1, r_2, \dots, r_N\}$ of the same size, which is drawn from a Gaussian distribution independently and randomly.

We construct the similarity kernels \mathbf{K}_f and \mathbf{K}_r of the features \mathbf{f} and noise sample set \mathbf{r} as the following decomposition proposed in [12]: $\mathbf{K}_f = \phi(\mathbf{f})^\top \phi(\mathbf{f})$ and $\mathbf{K}_r = \phi(\mathbf{r})^\top \phi(\mathbf{r})$, where all $\phi(f_i) \in \phi(\mathbf{f})$ and $\phi(r_i) \in \phi(\mathbf{r})$ are the ℓ_2 normalized vectors that guarantees the similarity kernels \mathbf{K}_f and \mathbf{K}_r to be real positive semidefinite matrices. The main idea of our SCI is to learn a similarity kernel \mathbf{K}_f of feature \mathbf{f} and make it less than the similarity kernel \mathbf{K}_r of random data \mathbf{r} . In this way, we keep the correlation among the features of synthetic samples lower than that among random vectors, thus alleviating the homogenization of synthetic data. Since matching two similarity kernels directly is an unconstrained optimization problem [28], we construct the loss using the major characteristics: eigenvalues and eigenvectors of kernels. Hence, our SCI loss term is defined as follows:

$$l_{SCI} = \max \left(\sum_i \left(\|\lambda_f^i - \lambda_r^i\|_2 - \hat{\lambda}_f^i \cos(v_f^i, v_r^i) \right), 0 \right), \quad (9)$$

where λ_f^i and λ_r^i are the i^{th} eigenvalues of \mathbf{K}_f and \mathbf{K}_r , respectively. v_f^i and v_r^i are the eigenvectors, and $\hat{\lambda}_f^i$ is the min-max normalized version of the eigenvalues applied to alleviate the effect of noisy structures.

3.4 Specific Quantization Scenarios

In view of specific application scenarios, including PTQ and QAT, our DSG scheme can be flexibly customized to adapt to different cases. We derive two typical examples from the original scheme for generative data-free PTQ and QAT, respectively (Fig. 4). In the following, we elaborate on the details about the two types of instances.

3.4.1 Post-training Quantization

In the data-free PTQ, based on the analysis in Fig. 2, our DSG focuses on alleviating homogenization at the distribution level, and the sample-level homogenization from the statistical perspective. Therefore, we combine the proposed SDA and LSE techniques to optimize the data generation process jointly. Suppose that for a network with N BN layers, we first apply SDA to each layer for relaxed loss terms \mathbf{l}_{SDA} , and then integrate LSE to enhance specific layers for every sample in the batch. Therefore, the overall loss $\mathcal{L}_{DSG-PTQ}$ can be defined as follows involving the above techniques:

$$\mathcal{L}_{DSG-PTQ} = (\mathbf{X}_{LSE}\mathbf{l}_{SDA})^T \mathbf{1}. \quad (10)$$

In addition to slack constraints for matching BN statistics, LSE provides layerwise enhancement and thus further diversifies the synthetic data.

Algorithm 1: The process of DSG scheme in PTQ

Input: pretrained model M with N BN layers, training iterations T .
Output: synthetic data: \mathbf{x}^s , quantized network Q .
Initialize \mathbf{x}^s from Gaussian distribution $\mathcal{N}(0, 1)$;
Initialize \mathbf{x}^0 from Gaussian distribution $\mathcal{N}(0, 1)$;
Get μ_i and σ_i from BN layers of M , $i = 1, 2, \dots, N$;
Forward propagate $M(\mathbf{x}^0)$ and gather activations;
Compute δ_i and γ_i using Eq. (6);
for all $t = 1, 2, \dots, T$ **do**
 Forward propagate $M(\mathbf{x}^s)$ and gather activations;
 Get $\tilde{\mu}_i^s$ and $\tilde{\sigma}_i^s$ from activations;
 Compute all l_{SDA_i} using Eq. (5);
 Descend $\mathcal{L}_{\text{DSG-PTQ}}$ using Eq. (10) and update data \mathbf{x}^s ;
Get synthetic data \mathbf{x}^s ;
Calibrate quantized network Q using data \mathbf{x}^s .

We relax constraints in matching BN statistics to bring more possibilities for the generation process. Meanwhile, we reinforce the loss of a specific layer to introduce attention for every single sample. As a result, the DSG scheme mitigates the homogenization issue in two different scales and thus generates diversified samples compared with existing methods. Finally, we use the synthetic data to calibrate the quantized network. Our DSG in PTQ is elaborated in Algorithm 1, and it is summarized in Fig. 4 as the case (a).

3.4.2 Quantization-aware Training

For the data-free QAT, based on the analysis in Section 3.2 and Fig. 2, existing generative methods suffer homogenization at the distribution level, and also at the sample-level homogenization from both statistical and spatial perspective. Therefore, our DSG applies the SDA, LSE, and SCI techniques jointly in QAT to diversify the synthetic data.

We first determine the optimization objectives for the generator G and the quantized network Q in the DSG scheme. As shown in Eq. (3), the optimization objectives in generative data-free QAT include: (1) training generator G to synthesize better data \mathbf{x}^s ; (2) finetuning the quantized network Q with synthetic data \mathbf{x}^s to improve accuracy. These two optimization goals are coupled, which leads to the high dependence of the performance of quantized network on the synthetic data. Therefore, for DSG in QAT, we apply an alternating optimization strategy to update the generator G and the quantized network Q .

Optimization for the generator G . We train the generator G to exploit the knowledge in the pre-trained full-precision network M , supervising the generator by the information of both its BN statistics and prediction probability. As shown in the Eq. (2), we initialize a set of random noise samples $\mathbf{z} \sim \mathcal{N}(0, 1)$ and specified labels \mathbf{y} , and feed it in generator G to synthesize the data \mathbf{x}^s and train the generator G . The loss function $\mathcal{L}_{\text{DSG-QAT}}$ for the generator can be express as

$$\mathcal{L}_{\text{DSG-QAT}} = \alpha (\mathbf{X}_{\text{LSE}} \mathbf{l}_{\text{SDA}})^T \mathbf{1} + \beta \mathbf{l}_{\text{SCI}}^T \mathbf{1} + \mathbb{E}_{G(\mathbf{z}), \mathbf{y}} [\text{CE}(M(G(\mathbf{z})), \mathbf{y})], \quad (11)$$

where CE is the cross-entropy loss between the label \mathbf{y} and the prediction for \mathbf{x} of the full-precision network M , which constrains the synthetic data to the specified label utilizing the well-trained full-precision network. α and β are trade-off parameters. $\mathbf{l}_{\text{SCI}} = [l_{\text{SCI}_0}, l_{\text{SCI}_1}, \dots, l_{\text{SCI}_B}]^T$ in Eq. (11) is the SCI loss terms for intermediate features of each blocks (B blocks in total) in generator

Algorithm 2: The process of DSG scheme in QAT

Input: pretrained model M with N BN layers, training iterations T .
Output: generator network G , quantized network Q .
Initialize \mathbf{z} from Gaussian distribution $\mathcal{N}(0, 1)$ and specify label \mathbf{y} ;
Get μ_i and σ_i from BN layers of M , $i = 1, 2, \dots, N$;
Forward propagate $M(\mathbf{z})$ and gather activations;
Compute δ_i and γ_i using Eq. (6);
for all $t = 1, 2, \dots, T$ **do**
 Generate the synthetic data $(\mathbf{x}^s, \mathbf{y})$ and gather activations;
 Forward propagate $M(\mathbf{x}^s)$ and gather activations;
 Descend $\mathcal{L}_{\text{DSG-QAT}}$ using Eq. (11) and update G ;
 Update the quantized network Q using data $(\mathbf{x}^s, \mathbf{y})$;
Get trained generator network G and finetuned quantized network Q .

G . This loss makes the generator G to exploit the knowledge in the pre-trained full-precision network M , supervising the generator by the information of both its BN statistics and prediction probability.

Optimization for the quantized network Q . In the finetuning process of the quantized network Q , we optimize the quantized network according to the usual practice [44]. Specifically, the data \mathbf{x}^s synthesized by generator G is applied to optimize the quantized network Q . The error of the quantized network Q is reduced to the generated data (\mathbf{x}, \mathbf{y}) and let the prediction probability distribution of Q close to the original full-precision network M , and thereby improving the performance of the quantized network.

In the optimization process, we train the generator G and quantized network Q alternately in every epoch, and the pre-trained full-precision network M is fixed. In this way, we fully exploit the knowledge in the pre-trained full-precision network to improve the quality of the synthetic data and the accuracy of the quantized network. Our DSG in QAT is elaborated in Algorithm 2 and is further illustrated in Fig. 4 as the case (b).

3.5 Analysis and Discussion

The techniques in our DSG scheme, SDA, LSE, and SCI, alleviate the homogenization of synthetic data at the distribution level and sample level. In Fig. 2, we statistically observe the behavior of the three types of data, i.e., data generated by our DSG scheme, data generated by other SOTA generative data-free quantization methods and real data. Here we analyze and discuss the effect of our DSG scheme in diversifying synthetic data in generative data-free quantization methods.

We first analyze the synthetic data generated by our DSG scheme in PTQ. Compared with the data generated by the existing generative data-free PTQ method (ZeroQ), the behavior of samples generated with our DSQ is more similar to that of real data statistically. As shown in Fig. 2(a), the distribution of our DSG data does not strictly fall in close vicinity to BN mean and standard deviation, instead, they are more various in value and thus more fluctuate in frequency. As introduced in Section 3.2, the Wasserstein distance between BN statistics and our DSG synthetic data is 0.124 (compared with 0.040 of ZeroQ). And in Fig. 2(c), the statistics of the data generated by ZeroQ are centralized, while that of the DSG samples are dispersed. The phenomenon means that our synthetic data significantly alleviates the sample-level homogenization of existing data-free generative PTQ methods from the statistical perspective. As mentioned in Section 3.2, we calculate the variance of the statistics of our DSG data and compare it with ZeroQ in

PTQ, which is 0.029 vs. 0.009. Fig. 2(e) presents the distribution of different types of synthetic data in the sample space, which shows that the behavior of our DSG samples in the sample space is close to real data and Gaussian data, that is, no additional sample-level homogenization from the spatial perspective. Considering the additional computational overhead, we combine SDA and LSE for the DSG scheme in the PTQ scenario.

For the DSG scheme in QAT, due to the utility of SDA and LSE, the distribution of our DSG data is not constrained strictly and the synthetic samples enjoy more diverse statistics, as Fig. 2(b) and Fig. 2(d) show. Additionally, the proposed SCI can further weaken the correlation among samples by constructing unsupervised loss for intermediate features in the generation process to alleviate the homogenization of the generated samples in sample space. From Fig. 2(f), we observe that the spatial homogenization of the synthesized samples existing in the method (GDFQ) is alleviated significantly by our DSG scheme. The density index near the cluster center of the synthesized sample generated by DSG is only 1449, which is even lower than that of real data 1681 and much lower than GDFQ 2052.

Therefore, the data generated by our DSG are more comprehensively diverse from various perspectives, which may have the potential to be an alternative in some quantization scenarios that real data is not accessible.

4 EXPERIMENTS

In this section, we conduct comprehensive experiments to validate the performance of our DSQ scheme on image classification tasks. We first conduct an ablation study to show the effects of different components, including SDA, LSE, and SCI in Section 4.1. Then in Section 4.2, we compare DSQ with SOTA data-free PTQ and QAT methods respectively across various network architectures. We evaluate the DSG on CIFAR10 [26] and ImageNet (ILSVRC12) [10] datasets in PTQ while on ImageNet dataset in QAT. Finally, in Section 4.3, we conduct a further study on synthetic data. Specifically, we analyze and discuss the data diversity, and integrate and evaluate our synthetic data with various calibration methods and data-driven quantization methods. The results show that good diversity is an important property of high-quality synthetic data.

DSG scheme. In the data-free PTQ, the proposed DSG scheme is used for generating synthetic data for calibration, and the effectiveness is evaluated by measuring the accuracy of quantized models. For the DSG scheme in QAT, we train the generator network to synthesize the data and use it to finetune the quantized network. Note that the generator in the DSG scheme in QAT is constructed following ACGAN [36].

Network architectures. We evaluate our DSG scheme in a wide range of network architectures with various bit-width to prove the versatility of our method. We employ VGG16bn [45], ResNet20/18/50 [21], SqueezeNext [15], InceptionV3 [48], ShuffleNet [60], and MobileNetV2 [43] with various bit-widths, including W4A4 (means 4-bit weight and 4-bit activation), W6A6, W8A8, etc.

Implementation details. The proposed scheme is implemented by PyTorch for the sake of the powerful automatic differentiation mechanism. We adopt Gaussian distribution as initialization for the data generation process in our DSG scheme. In our experiments, we quantize all the layers. And the activation is clipped in a layerwise manner. As for hyper-parameter (e.g., the number of

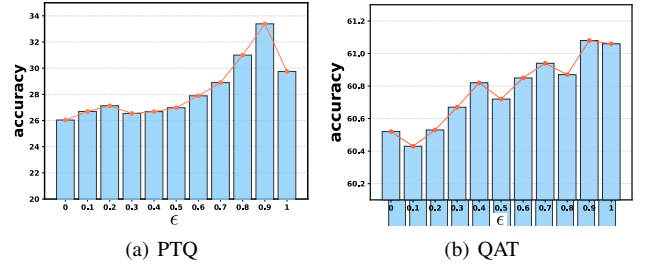


Fig. 5: The accuracy comparison of different ϵ values in Eq. (6) on ResNet18 in PTQ and QAT. As ϵ varies from 0 to 0.9, the final accuracy is mainly on the rise. But a significant drop is caused by the outliers when $\epsilon = 1$

Method	No FT	W-bit	A-bit	Top-1
Baseline	–	32	32	71.47
Vanilla (ZeroQ)	✓	4	4	26.04
Sample Correlation Inhibition	✓	4	4	26.09
Layerwise Sample Enhancement	✓	4	4	27.12
Slack Distribution Alignment	✓	4	4	33.39
DSG (Ours)	✓	4	4	34.53
Vanilla (GDFQ)	✗	4	4	60.52
Layerwise Sample Enhancement	✗	4	4	60.71
Sample Correlation Inhibition	✗	4	4	60.92
Slack Distribution Alignment	✗	4	4	61.08
DSG (Ours)	✗	4	4	61.58

TABLE 1: Ablation study for DSG scheme on ResNet18. We abbreviate quantization bits used for weights as "W-bit" (for activations as "A-bit"), top-1 test accuracy as "Top-1"

iterations to provide synthetic data), we mostly follow the released official implementations or the models and settings clarified in their original paper for a fair comparison. For the training and finetuning process of DSG in QAT, we use the Adam and SGD optimizer in the experiments, where momentum is 0.9 and weight decay is $1e-4$. The α and β in Eq. (11) are set as $1e-1$ and $1e2$ after a simple grid search. In addition, we train the generator and the quantized network for 200 epochs. The learning rates are initialized to $1e-3$ and $1e-4$, respectively, and are decayed to $1e-4$ and $1e-5$ at the 100th epoch.

4.1 Ablation Study

We investigate the effect of the proposed LSE, SDA, and SCI techniques for our DSG scheme in data-free PTQ and QAT by ablation experiments. We use the ResNet18 architecture with the ImageNet dataset to evaluate our method under the W4A4 bit-width setting, which can show the effect of each part more obviously.

4.1.1 Effect of SDA

We first analyze the effectiveness of SDA. As discussed earlier, hyper-parameter ϵ determines the degree of relaxation in SDA. Therefore, in Fig. 5, we verify the impact of different values of ϵ in the interval $(0, 1]$ with a moderate step size 0.1, and further add $\epsilon = 0$ to serve as the vanilla case that the fitting of BN statistics is constrained without relaxation. In PTQ (Fig. 5(a)), when the ϵ varies from 0 to 0.9, the final performance increases gradually from 26.04% to 33.39%. In QAT (Fig. 5(b)), the accuracy also presents an overall upward trend (from 60.52% to 61.08%) as the ϵ varies

from 0 to 0.9. However, when $\epsilon = 1$, the accuracy drops more or less in both scenarios, which is 3.61% in PTQ and 0.02% in QAT. These phenomena forcefully prove that by way of relaxing the constraints, the SDA method brings generated data a certain offset when fitting the BN statistic distribution, which contributes to feature diversity and consequently improves the performance. And when ϵ is set to 1, the degree of slack reaches the limit as all the outliers in $\tilde{\mu}_i^0$ and $\tilde{\sigma}_i^0$ are taken into account, which means the feature distribution of generated data might be out of the reasonable range. Therefore, it might result in better feature diversity in synthetic data but would harm the final accuracy of the quantized network. Therefore, we set the default value of ϵ as 0.9 empirically to balance divergence and the impact of outliers.

As the results shown in TABLE 1, the vanilla data-free PTQ method without SDA suffers a severe accuracy degradation by 7.41% compared to the whole DSG, and the SDA also provides 0.56% accuracy promotion in data-free QAT (vanilla 60.52% vs. SDA 61.08%). The results reflect that SDA is essential. Compared to the other two parts of our scheme, SDA may provides a major contribution to the final performance.

4.1.2 Effect of LSE

The TABLE 1 also shows that LSE can improve the performance in both data-free QAT and PTQ. As the ablation results show, in PTQ, LSE method gives a non-negligible increment compared with ZeroQ by 1.08%. As for in QAT, it also helps the DSG scheme to have a slight improvement compared with the vanilla method by 0.19%. Moreover, the results for PTQ in TABLE 1 present that the LSE and SDA are orthogonal in our DSG scheme, jointly optimizing the quantized network. In PTQ, the whole scheme including these two techniques surpasses vanilla competitors by a notable 8.49%.

4.1.3 Effect of SCI

Then we evaluate SCI in data-free quantization. In the previous analysis of Fig. 2, we present that spatial homogenization exists in the synthetic data of the generative data-free QAT methods, so the motivation of our SCI is to alleviate the sample-level homogenization from the spatial perspective. TABLE 1 shows the effects of using SCI. In QAT, compared with the vanilla method, integrating with SCI helps to acquire better accuracy, which is 0.40% higher. And the application of SCI in PTQ achieves few performance gains (only 0.05%), which also verifies our previous observation that the vanilla data-free PTQ method (ZeroQ) does not seem to cause obvious spatial homogenization, so optimizing the synthetic samples from the spatial perspective has just little effect. The results show that the proposed SCI alleviates the sample-level homogenization from the spatial perspective and improves performance significantly in generative data-free QAT.

Intuitively, these techniques are motivated by different observations, and also the processes are carefully engineered that they hardly interfere with each other. In short, SDA and LSE improve the loss related to BN statistics, aiming to prevent the generated samples from overfitting to BN statistics and makes the samples focus on the statistics of different layers. While the SCI for data-free QAT constructs an unsupervised loss to constrain the features in the generator to holding distances among them, so that mitigate the sample homogenization. The results show that, in the data-free QAT, DSG scheme equipped with these three techniques obtains 1.06% improvement in total with ResNet18 under W4A4 setting, which is up to 61.58%.

Arch	Method	No D	No FT	W-bit	A-bit	Top-1	
ResNet20	Baseline	-	-	32	32	94.08	
	Real Data	✗	✓	4	4	87.38	
	ZeroQ	✓	✓	4	4	85.39	
	DSG (Ours)	✓	✓	4	4	87.75	
	Real Data	✗	✓	6	6	93.80	
	ZeroQ	✓	✓	6	6	93.33	
	DSG (Ours)	✓	✓	6	6	93.79	
	Real Data	✗	✓	8	8	93.95	
	ZeroQ	✓	✓	8	8	93.94	
	DSG (Ours)	✓	✓	8	8	94.07	
	VGG16bn	Baseline	-	-	32	32	93.86
		Real Data	✗	✓	4	4	92.50
ZeroQ		✓	✓	4	4	91.79	
DSG (Ours)		✓	✓	4	4	92.89	
Real Data		✗	✓	6	6	93.48	
ZeroQ		✓	✓	6	6	93.45	
DSG (Ours)		✓	✓	6	6	93.68	
Real Data		✗	✓	8	8	93.59	
ZeroQ		✓	✓	8	8	93.53	
DSG (Ours)		✓	✓	8	8	93.61	

TABLE 2: Results of data-free PTQ methods with ResNet20 and VGG16bn on CIFAR10

4.2 Comparison with SOTA Methods

We extensively evaluate our DSG scheme on a wide range of architectures on CIFAR10 and ImageNet datasets for the image classification tasks. We denote the bit-width setting of the quantized network as $WwAa$ where w is the bit-width for weight and a is that for activation, like W8A8, W6A6, W4A4, etc.

4.2.1 Comparison with Data-free PTQ Methods

To evaluate the advantage of the proposed scheme in PTQ, we first compare our DSG against other data-free PTQ methods (ZeroQ [5], DFQ [35], ACIQ [1], MSE [7], KL [46], and OCS [61]) on CIFAR10 and ImageNet datasets. Among these methods, ZeroQ is a generative data-free PTQ method, which reconstructs synthetic data to calibrate the quantized network, while others use weight equalization or analytical clip range to improve the network performance. Besides, we additionally compare our method with OCS, which is also a PTQ method but requires real data for calibration. We evaluate these methods on various bit-width settings, and the results on CIFAR10 and ImageNet dataset are shown as TABLE 2 and TABLE 3, respectively.

Specifically, on CIFAR10 [26] dataset, we evaluate our DSG with ResNet20 [22] and VGG16bn [45]. The results are shown in TABLE 2. Under all settings on the CIFAR10 dataset, our DSG far exceeds existing SOTA methods. And we highlight that the quantized network calibrated with DSG data completely surpasses the network calibrated with real data on various settings. For example, under the W4A4 settings of ResNet20 and VGG6bn, our method exceeds the calibration with real data by 0.37% and 0.39%, respectively.

(a) ResNet18 and ResNet50							(b) SqueezeNext, InceptionV3, and ShuffleNet						
Arch	Method	No D	No FT	W-bit	A-bit	Top-1	Arch	Method	No D	No FT	W-bit	A-bit	Top-1
ResNet18	Baseline	–	–	32	32	71.47	SqueezeNext	Baseline	–	–	32	32	69.38
	Real Data	✗	✓	4	4	31.86		Real Data	✗	✓	6	6	62.88
	DFQ	✓	✓	4	4	0.10		ZeroQ	✓	✓	6	6	39.83
	ACIQ	✓	✓	4	4	7.19		DSG (Ours)	✓	✓	6	6	60.50
	MSE	✓	✓	4	4	15.08		Real Data	✗	✓	8	8	69.23
	KL	✓	✓	4	4	16.27		ZeroQ	✓	✓	8	8	68.01
	ZeroQ	✓	✓	4	4	26.04		DSG (Ours)	✓	✓	8	8	69.27
	DSG (Ours)	✓	✓	4	4	34.53		Baseline	–	–	32	32	78.80
	Real Data	✗	✓	6	6	70.62		Real Data	✗	✓	4	4	23.23
	ACIQ	✓	✓	6	6	61.15		ZeroQ	✓	✓	4	4	12.00
	KL	✓	✓	6	6	61.34	DSG (Ours)	✓	✓	4	4	34.89	
	MSE	✓	✓	6	6	66.96	InceptionV3	Real Data	✗	✓	6	6	77.96
	DFQ	✓	✓	6	6	67.30		ZeroQ	✓	✓	6	6	75.14
	ZeroQ	✓	✓	6	6	69.74		DSG (Ours)	✓	✓	6	6	76.52
	DSG (Ours)	✓	✓	6	6	70.46		Real Data	✗	✓	8	8	78.78
	Real Data	✗	✓	8	8	71.44		ZeroQ	✓	✓	8	8	78.70
	ACIQ	✓	✓	8	8	68.78		DSG (Ours)	✓	✓	8	8	78.81
	DFQ	✓	✓	8	8	69.70		Baseline	–	–	32	32	65.07
	KL	✓	✓	8	8	70.69		Real Data	✗	✓	6	6	44.75
	MSE	✓	✓	8	8	71.01		ZeroQ	✓	✓	6	6	39.92
ZeroQ	✓	✓	8	8	71.43	DSG (Ours)		✓	✓	6	6	44.88	
DSG (Ours)	✓	✓	8	8	71.49	Real Data	✗	✓	8	8	64.52		
ResNet50	Baseline	–	–	32	32	77.72	ShuffleNet	ZeroQ	✓	✓	8	8	64.46
	Real Data	✗	✓	4	4	22.10		DSG (Ours)	✓	✓	8	8	64.77
	ZeroQ	✓	✓	4	4	8.20		Baseline	–	–	32	32	65.07
	DFQ	✓	✓	4	4	10.32		Real Data	✗	✓	6	6	44.75
	DSG (Ours)	✓	✓	4	4	23.10		ZeroQ	✓	✓	6	6	39.92
	Real Data	✗	✓	6	6	75.52		DSG (Ours)	✓	✓	6	6	44.88
	OCS	✗	✓	6	6	74.80		Real Data	✗	✓	8	8	64.52
	ZeroQ	✓	✓	6	6	75.56		ZeroQ	✓	✓	8	8	64.46
	DSG (Ours)	✓	✓	6	6	76.07		DSG (Ours)	✓	✓	8	8	64.77
	Real Data	✗	✓	8	8	77.70		Baseline	–	–	32	32	65.07
	ZeroQ	✗	✓	8	8	77.67	Real Data	✗	✓	6	6	44.75	
	DSG (Ours)	✓	✓	8	8	77.68	ZeroQ	✓	✓	6	6	39.92	

TABLE 3: Results of data-free PTQ methods with (a) ResNet18, ResNet50, (b) SqueezeNext, InceptionV3, and ShuffleNet on ImageNet. Here, "Arch" means the network architectures, "No D" means that none of the data is used to assist quantization, "No FT" stands for no finetuning (retraining). "Real Data" represents using real training data and quantization methods in ZeroQ (without any finetuning)

As listed in TABLE 3, the results over various network architectures, including ResNet18/50 [21], SqueezeNext [15], InceptionV3 [48], and ShuffleNet [60], demonstrate that our proposed DSG significantly outperforms previous sample generation methods. As the results shown, the accuracy of quantized networks calibrated with our DSG data under the W8A8 setting is almost not decreased and even surpasses the full-precision (W32A32) baseline networks on the ResNet18 and InceptionV3 architectures. The higher accuracy might be attributed to making full use of the potential of the quantized network. Quantizing the network to W8A8 maintains greater representation ability of the network compared with the lower bit-width quantization (such as W4A4) and brings less quantization error. Thus, under this setting, our diversified data can alleviate the performance degradation of the network quantization while even leading to a better solution

compared with the full-precision network. And the advantage of our DSG gets more evident when the bit-width becomes lower. For example, our DSG outperforms ZeroQ on SqueezeNext on the W6A6 setting by more than 20%, and even outperforms real data by a slight 0.13%. And it is noteworthy that in W4A4 cases with ResNet18 architecture, our DSG surpasses ZeroQ by 8.49%, and even surpasses real data by a notable 2.67%, which is up to 34.53%. Moreover, with InceptionV3 under W4A4 settings, our DSG helps to acquire 34.89% accuracy, which is much higher than ZeroQ and real data by eminent 22.89% and 11.66% respectively.

4.2.2 Comparison with Data-free QAT Methods

Furthermore, to demonstrate the applicability of our DSG scheme in data-free QAT, we compare it with existing QAT methods, such as DFC [19], RVQuant [38], Integer-Only [24], ZAQ [32],

(a) ResNet18 and ResNet50							(b) ShuffleNet, MobileNetV2, and InceptionV3								
Arch	Method	No D	No FT	W-bit	A-bit	Top-1	Arch	Method	No D	No FT	W-bit	A-bit	Top-1		
ResNet18	Baseline	–	–	32	32	71.74	ShuffleNet	Baseline	–	–	32	32	65.07		
	GDFQ	✓	✗	4	4	60.52		GDFQ	✓	✗	4	4	21.78		
	DSG (Ours)	✓	✗	4	4	61.58		DSG (Ours)	✓	✗	4	4	28.11		
	Integer-Only	✗	✗	6	6	67.30		GDFQ	✓	✗	6	6	60.12		
	GDFQ	✓	✗	6	6	70.43		DSG (Ours)	✓	✗	6	6	61.32		
	DSG (Ours)	✓	✗	6	6	70.83		GDFQ	✓	✗	8	8	64.03		
	DFC	✓	✗	8	8	69.57		DSG (Ours)	✓	✗	8	8	64.51		
	RVQuant	✗	✗	8	8	70.01		Baseline	–	–	32	32	71.88		
	GDFQ	✓	✗	8	8	71.43		GDFQ	✓	✗	4	4	51.30		
	DSG (Ours)	✓	✗	8	8	71.43		DSG (Ours)	✓	✗	4	4	54.66		
	ResNet50	Baseline	–	–	32	32		77.72	MobileNetV2	GDFQ	✓	✗	6	6	70.98
		GDFQ	✓	✗	4	4		55.65		DSG (Ours)	✓	✗	6	6	71.22
RVQuant		✗	✗	4	4	64.90	GDFQ	✓		✗	8	8	70.17		
ZAQ		✓	✗	4	4	70.06	ZAQ	✓		✗	8	8	71.43		
DSG (Ours)		✓	✗	4	4	70.12	DSG (Ours)	✓		✗	8	8	72.89		
GDFQ		✓	✗	6	6	76.59	Baseline	–		–	32	32	78.80		
DSG (Ours)		✓	✗	6	6	77.10	GDFQ	✓		✗	4	4	70.39		
GDFQ		✓	✗	8	8	77.51	DSG (Ours)	✓		✗	4	4	71.72		
DSG (Ours)		✓	✗	8	8	77.62	GDFQ	✓		✗	6	6	77.20		
InceptionV3		Baseline	–	–	32	32	77.72	DSG (Ours)		✓	✗	6	6	78.51	
		GDFQ	✓	✗	4	4	60.52	GDFQ		✓	✗	8	8	78.62	
		DSG (Ours)	✓	✗	4	4	61.58	DSG (Ours)		✓	✗	8	8	78.94	
	Integer-Only	✗	✗	6	6	67.30	Baseline	–	–	32	32	71.88			
	GDFQ	✓	✗	6	6	70.43	GDFQ	✓	✗	4	4	51.30			
	DSG (Ours)	✓	✗	6	6	70.83	DSG (Ours)	✓	✗	4	4	54.66			
	DFC	✓	✗	8	8	69.57	GDFQ	✓	✗	6	6	70.98			
	RVQuant	✗	✗	8	8	70.01	DSG (Ours)	✓	✗	6	6	71.22			
	GDFQ	✓	✗	8	8	71.43	GDFQ	✓	✗	8	8	70.17			
	DSG (Ours)	✓	✗	8	8	71.43	ZAQ	✓	✗	8	8	71.43			

TABLE 4: Results of data-free QAT methods with ResNet18, ResNet50, InceptionV3, ShuffleNet, and MobileNetV2 on ImageNet

and GDFQ [44]. These methods are engineered to finetune and update the network parameters. DFC is a finetuning method to recover accuracy for ultra-low bit-width cases, which uses Inceptionism [33] to facilitate the generation of data with random labels. The other mentioned methods finetune the quantized network to improve the accuracy of the network. Among them, ZAQ and GDFQ introduce a generator to synthesize data and use the generated data to finetune the network. We evaluate these methods on various bit-width settings in the more challenging large-scale image classification task. The results on ImageNet are shown as TABLE 4.

We test these methods on ResNet18/50 [21], InceptionV3 [48], ShuffleNet [60], and MobileNetV2 [43]. The results in TABLE 4 show that our DSG enjoys the best performance. Concretely, as can be seen, regardless of network architecture, our DSG method surpasses many previous methods, including DFC, RVQuant, Integer-Only, and GDFQ in various bit-width settings. And it is noteworthy that, after finetuning with our DSG data, quantized ResNet18 and InceptionV3 even surpass their full-precision counterparts under the W8A8 setting. But the improvement is more obvious in lower bit-width settings, such as 4-bit, our DSG scheme outperforms real data by up to 11.66% with InceptionV3, and that by 2.67% with ResNet18. Comparing with other data-free QAT training methods, our DSG outperforms GDFQ by 1.06% and 12.81% with ResNet18 and ResNet50 respectively, also higher than RVQuant by 3.56% with ResNet50. Besides the mainstream neural architectures, we also evaluate our DSG over existing well-designed lightweight architectures. The proposed DSG shows

an overwhelming advantage over GDFQ with a similar training pipeline, 20.67% higher with SqueezeNext, 4.96% higher with ShuffleNet in a W6A6 setting, and 22.89% higher with InceptionV3 in the W4A4 setting.

In short, our DSG scheme outperforms other competitors over a wide range of experiments in data-free PTQ and QAT, including various bit-width, different network architectures, and two datasets. All the results forcefully demonstrate that the diversity of generated data is significant to calibrate the model for higher accuracy, especially in ultra-low bit-width conditions. If the synthetic data are homogeneous or even identical at the distribution and sample level, it would be ineffectual when used to quantize the network. Our DSG effectively diversifies the synthetic data and thus improves the performance of the quantized network.

4.3 Further Study on Synthetic Data

To further demonstrate the data diversifying caused by our DSG scheme has a general gain to the quantized network, we provide more experiments as corroborations to support our viewpoint. In our paper, we have conducted a bunch of experiments on our synthetic data to evaluate its effectiveness in improving the network performance, including analyzing the data diversity and integrating the synthetic data generated by our method to different calibration methods and data-driven quantization methods. The experiments show that benefits by the increase in the diversity of synthetic data, the network performance in various methods is significantly improved. It shows that good diversity is an important property of high-quality synthetic data.

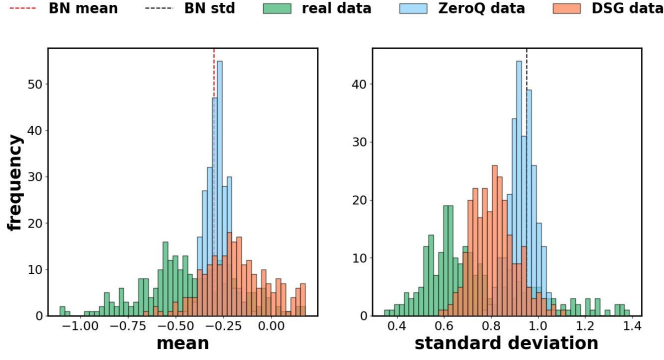


Fig. 6: Mean and standard deviation of the activations in one channel of ResNet18 when feeding different types of data (with 256 samples), including the synthetic data generated by ZeroQ and DSG and the real data. Each sample generated by ZeroQ behaves similarly overfitting BN statistics compared with real data, which shows the homogenization at both distribution and sample level. Our DSG data enjoys the diversity close to real data to obtain the accurate quantized network

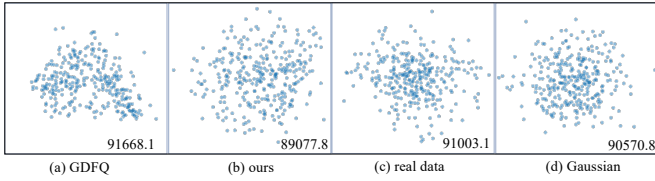


Fig. 7: Visualization of samples generated by (a) GDFQ method, (b) our SCI method, and (c) real data, (d) Gaussian random data. We collect 512 samples for each type of data randomly and reduce dimensions with PCA. Samples generated by our SCI method are more scattered than GDFQ samples and close to that of real data

4.3.1 Analysis and Discussion for Data Diversity

In this section, we further discuss the visualization results of our DSG scheme. First, for data-free PTQ, we show the distribution of statistics of the real data, vanilla data (ZeroQ), and DSG data (ours) in Fig. 6, which explains that SDA and LSE alleviate the homogenization from the aforementioned two levels. Then, for data-free QAT, we visualized samples of vanilla data (GDFQ), DSG data (ours), real data, and Gaussian data in Fig. 7 to show the additional effect of SCI that diversifies samples by inhibiting feature correlation. We also visualize the synthetic samples of our method and other generative data-free quantization methods (ZeroQ, GDFQ) in Fig. 8 to visually show the effect of data diversifying.

In Fig. 6, it can be obviously investigated that DSQ samples behave more like real data than vanilla data on the offset of mean and standard deviation statistics, which corresponds to the diversity at the distribution level of our generated data scheme. Especially, the SDA plays an important role to make the distribution diverse by slacking the constraint of statistics during the generation process. This phenomenon proves that our DSG scheme diversifies the synthetic data at the distribution level. Moreover, the DSG scheme also generates data with a larger variance compared to the vanilla scheme, which implies that our data samples are widely dispersed and more in line with the real situation. Especially, both SDA and LSE jointly promote diversity at the sample level, which might be useful in providing more content information.

The motivation of the SCI method is to inhibit the correlation among features in the generator, and thus the synthetic samples are separated, as shown in Fig. 7. We visualize the data generated by

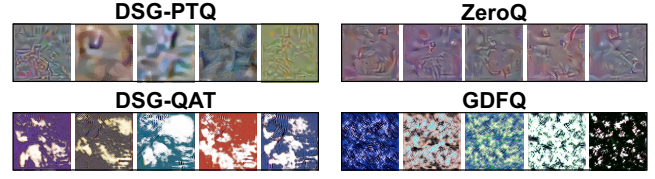


Fig. 8: Visualization of synthetic data for ZeroQ, GDFQ, and our DSG method in PTQ and QAT scenario. Each showcases 5 examples

the vanilla method (GDFQ) and our SCI method, as well as the real data and Gaussian random data. At the right-bottom corner of each subplot, we measure the diversity of each set of features by summarizing the elements in the similarity kernel \mathbf{K}_f as an index $s = \sum_{i,j \in \mathbf{f}_k} [\mathbf{K}_{i,j}]$, which indicates the feature distance between samples in spatial perspective. The larger the s , the more similar the samples. As can be seen from Fig. 7, the Gaussian random data is dispersive and stochastic. And it is also quite obvious that the real data is naturally distinct. However, samples generated by the vanilla GDFQ method, as shown in the subplot (a), are generally more concentrated in comparison, some of which are even overlapped. So it has the biggest s . Instead, our SCI utilizes the random Gaussian data as initialization and inhibits the correlation between samples to make the data more dispersed than Gaussian sampling. The samples generated by our method, which has the smallest s , are more dispersed than those generated by the vanilla method and seem close to real data. It demonstrates that the SCI method helps to avoid homogenization from the spatial perspective, and thus diversifies the synthetic samples from each other.

We visualize some synthetic samples of our method and other generative data-free quantization methods (ZeroQ, GDFQ). Take a closer look at Fig. 8, comparing pictures of DSG-PTQ and ZeroQ above, both of which generate images directly and update them iteratively. It is obvious that pictures generated by our DSG-PTQ method seem to have diverse colors with fine-grained textures and coarse-grained figures, while pictures of ZeroQ seem identical and have little difference in between. Meanwhile, below two sets of pictures are generated by DSG-QAT and GDFQ respectively. Owing to the generator, there are much more possibilities in the generation process and finally exhibit in both sets of images. It can be seen with naked eyes that samples of our DSG-QAT have distinct colors with higher saturation degrees, and white images inside the pictures have uncertain patterns. However, although samples generated by GDFQ have different colors and details inside the pictures as well, these samples have a uniform style in texture, which is tanglesome and poor in diversity.

4.3.2 Evaluation with Calibration Methods

Additionally, to verify the versatility and robustness of the performance gains of our DSG method, we evaluate our DSG scheme with different calibration methods and compare it with other data generation methods under the same setting. The calibration methods include Percentile, EMA, and MSE. As shown in TABLE 5, no matter which calibration methods is integrated, our DSG scheme substantially outstrips ZeroQ by 6.52%, 2.87% and 0.61% respectively. The results strongly suggest that DSG can achieve the leading performance in various experimental settings, and thus the improvement is versatile and robust for various calibration methods.

We also evaluate the synthetic data with DFQ [35], which is a calibration method for data-free quantization. Specifically,

Method	No D	W-bit	A-bit	Quant	Top-1
Baseline	–	–	32	32	71.47
Real Data	✗	4	4	Vanilla	31.86
ZeroQ	✓	4	4	Vanilla	26.04
DSG (Ours)	✓	4	4	Vanilla	34.53
Real Data	✗	4	4	Percentile	42.83
ZeroQ	✓	4	4	Percentile	32.24
DSG (Ours)	✓	4	4	Percentile	38.76
Real Data	✗	4	4	EMA	42.67
ZeroQ	✓	4	4	EMA	32.31
DSG (Ours)	✓	4	4	EMA	35.18
Real Data	✗	4	4	MSE	41.45
ZeroQ	✓	4	4	MSE	39.39
DSG (Ours)	✓	4	4	MSE	40.00

TABLE 5: Evaluation with calibration on ImageNet. We evaluate our DSG scheme with various calibration methods (Percentile, EMA, MSE) on ResNet18, and Vanilla means the calibration method adopted by ZeroQ, which simply obtain the quantizer by the maximum and minimum of the weight and activation

Method	No D	No FT	W-bit	A-bit	Top-1
Baseline	–	–	32	32	69.76
Real Data	✗	✓	6	6	59.16
ZeroQ	✓	✓	6	6	58.12
DSG (Ours)	✓	✓	6	6	58.69
Real Data	✗	✓	8	8	69.22
ZeroQ	✓	✓	8	8	65.75
DSG (Ours)	✓	✓	8	8	68.88

TABLE 6: Evaluation with DFQ on ImageNet. We use cross-layer equalization and bias correction proposed by DFQ to perform per-layer quantization on ResNet18

DFQ has proposed cross-layer range equalization to equalize the different channel ranges of weight in per-layer quantization and bias correction which is to eliminate the biased quantization error. Both of the two techniques rely on the statistics of BN layers following the convolution layer. Therefore, BN layers are needed to calibrate the corresponding activations, so they have to proceed behind each convolution layer, which results in DFQ only working on specific network architectures and cannot be commonly practiced. Fortunately, generative methods, such as ZeroQ and our DSG, can work on arbitrary architectures, and the statistics of activations can take the place of BN statistics and thus be used in the DFQ method. TABLE 6 shows the closeups of two generative data-free quantization methods, i.e., ZeroQ and DSG, in conjunction with the DFQ method. Results show that our DSG outperforms ZeroQ by 0.57% and 3.13% in W6A6 and W8A8 cases.

4.3.3 Evaluation with Data-driven Quantization Methods

Experiments above are conducted on calibration methods that optimize the clipping value for activations. We further evaluate our DSG data with a novel data-driven PTQ method named Adaround [34], which utilizes a rounding approach to quantize weights. Meanwhile, we introduce two other data generation tricks

Arch	Method	No D	Label	Prior	W-bit	A-bit	Top-1
ResNet18	Real Data	✗	✗	✗	3	32	64.16
	ZeroQ	✓	✗	✗	3	32	49.86
	DSG (Ours)	✓	✗	✗	3	32	56.09
	DSG (Ours)	✓	✓	✗	3	32	58.27
	DSG (Ours)	✓	✓	✓	3	32	61.32
	Real Data	✗	✗	✗	4	32	68.42
	ZeroQ	✓	✗	✗	4	32	63.86
	DSG (Ours)	✓	✗	✗	4	32	66.87
	DSG (Ours)	✓	✓	✗	4	32	67.09
	DSG (Ours)	✓	✓	✓	4	32	67.78
	Real Data	✗	✗	✗	5	32	69.21
	ZeroQ	✓	✗	✗	5	32	68.39
	DSG (Ours)	✓	✗	✗	5	32	68.97
	DSG (Ours)	✓	✓	✗	5	32	69.02
	DSG (Ours)	✓	✓	✓	5	32	69.16
	Real Data	✗	✗	✗	4	8	68.24
ZeroQ	✓	✗	✗	4	8	56.34	
DSG (Ours)	✓	✓	✓	4	8	62.40	
MobileNetV2	Real Data	✗	✗	✗	3	32	58.13
	ZeroQ	✓	✗	✗	3	32	11.07
	DSG (Ours)	✓	✓	✓	3	32	45.40
	Real Data	✗	✗	✗	4	32	68.37
	ZeroQ	✓	✗	✗	4	32	56.16
	DSG (Ours)	✓	✓	✓	4	32	58.13

TABLE 7: AdaRound on ImageNet with ResNet18 and MobileNetV2. We evaluate the DSG scheme on AdaRound, one of the SOTA methods of data-driven post-training quantization, which learns how to quantize weights using several batches of unlabeled samples. We adopt "Label" [20] and image prior ("Prior") [58] techniques to evaluating our DSG scheme further

into our DSG scheme, e.g., generating data with labels [20] provides class information from parameters, image prior [58] avoids generating unpractical scenes or unrecognizable patterns. We have conducted different bit-width for both weights and activations on different network architectures including ResNet18 and MobileNetV2 (TABLE 7). And we generate 1024 samples in every single experiment. TABLE 7 shows that our DSG scheme outperforms ZeroQ by a wide margin when solely quantizing weights and preserving full-precision for activations. It is notable that in ultra-low bit-width settings (i.e. 3-bit), our DSG surpasses ZeroQ by 11.46% on ResNet18 and a surprising 34.33% on MobileNetV2. We also tried quantizing activations to 8-bit, and the results prove that our DSG is more robust to quantization of parameters, which outstrips ZeroQ by 6.06% with ResNet18 on ImageNet. Besides, we have the observation that the model gains further improvements when these tricks are applied together, even close the performance applying real data. Because our DSG is orthogonal with labels and image prior methods, so these methods can jointly boost the accuracy performance without any inconsistency.

5 CONCLUSION

In this paper, we first revisit the sample generation process in generative data-free PTQ and QAT quantization and reveal

the homogenization of synthetic data in distribution and sample level. And then we propose a novel Diverse Sample Generation (DSG) scheme for generative data-free quantization, to address the deficiencies of previous methods which severely degrades the quality of the synthetic data and further harms the performance of the quantized network. Our scheme has been evaluated on a variety of bit-widths and neural architectures, and the results forcefully demonstrate the effectiveness and versatility of the DSG scheme. It shows notable accuracy improvements in ultra-low bit-width cases (e.g. W4A4), the most impressive of which is even high up to 22%. Moreover, benefiting from the enhanced diversity, the performance of the network is significantly improved in various methods integrating with synthetic data, which demonstrates that diversity is an important property of high-quality synthetic data.

6 ACKNOWLEDGEMENT

This work was supported by National Natural Science Foundation of China (62022009, 61872021), Beijing Nova Program of Science and Technology (Z191100001119050), State Key Lab of Software Development Environment (SKLSDE-2020ZX-06).

REFERENCES

- [1] R Banner, Y Nahshan, E Hoffer, and D Soudry. Post training 4-bit quantization of convolution networks for rapid-deployment. *CoRR, abs/1810.05723*, 2018. [9](#)
- [2] Ron Banner, Yury Nahshan, Elad Hoffer, and Daniel Soudry. Post-training 4-bit quantization of convolution networks for rapid-deployment, 2019. [1](#), [3](#)
- [3] Alexei Borodin. Determinantal point processes. *arXiv preprint arXiv:0911.1153*, 2009. [6](#)
- [4] Adrian Bulat and Georgios Tzimiropoulos. Hierarchical binary cnns for landmark localization with limited resources. *IEEE Transactions on Pattern Analysis and Machine Intelligence*, 42(2):343–356, 2020. [1](#)
- [5] Yaohui Cai, Zhewei Yao, Zhen Dong, Amir Gholami, Michael W Mahoney, and Kurt Keutzer. Zeroq: A novel zero shot quantization framework. In *Proceedings of the IEEE/CVF Conference on Computer Vision and Pattern Recognition*, pages 13169–13178, 2020. [1](#), [2](#), [3](#), [9](#)
- [6] Laming Chen, Guoxin Zhang, and Hannang Zhou. Fast greedy map inference for determinantal point process to improve recommendation diversity. In *Conference on Neural Information Processing Systems (NeurIPS)*, 2018. [6](#)
- [7] Tianqi Chen, Mu Li, Yutian Li, Min Lin, Naiyan Wang, Minjie Wang, Tianjun Xiao, Bing Xu, Chiyuan Zhang, and Zheng Zhang. Mxnet: A flexible and efficient machine learning library for heterogeneous distributed systems. *arXiv preprint arXiv:1512.01274*, 2015. [9](#)
- [8] Yoojin Choi, Jihwan Choi, Mostafa El-Khamy, and Jungwon Lee. Data-free network quantization with adversarial knowledge distillation, 2020. [1](#), [2](#), [3](#)
- [9] Yoni Choukroun, Eli Kravchik, Fan Yang, and Pavel Kisilev. Low-bit quantization of neural networks for efficient inference. In *2019 IEEE/CVF International Conference on Computer Vision Workshop (ICCVW)*, pages 3009–3018. IEEE, 2019. [1](#), [3](#)
- [10] Jia Deng, Wei Dong, Richard Socher, Li Jia Li, Kai Li, and Fei Fei Li. Imagenet: a large-scale hierarchical image database. In *Proceedings of the IEEE/CVF Conference on Computer Vision and Pattern Recognition (CVPR)*, 2009. [8](#)
- [11] Yueqi Duan, Jiwen Lu, Ziwei Wang, Jianjiang Feng, and Jie Zhou. Learning deep binary descriptor with multi-quantization. *IEEE Transactions on Pattern Analysis and Machine Intelligence*, 41(8):1924–1938, 2019. [1](#)
- [12] Mohamed Elfeki, Camille Couprie, Morgane Riviere, and Mohamed Elhoseiny. Gdpp: Learning diverse generations using determinantal point processes. In *International Conference on Machine Learning (ICML)*, 2019. [2](#), [6](#)
- [13] Mark Everingham, Luc Van Gool, Christopher K. I. Williams, John Winn, and Andrew Zisserman. The pascal visual object classes challenge. *International Journal of Computer Vision (IJCV)*, 2010. [1](#)
- [14] DF Frey and RA Pimentel. Principal component analysis and factor analysis. 1978. [2](#)
- [15] Amir Gholami, Kiseok Kwon, Bichen Wu, Zizheng Tai, Xiangyu Yue, Peter Jin, Sicheng Zhao, and Kurt Keutzer. SqueezeNEXT: Hardware-aware neural network design, 2018. [2](#), [8](#), [10](#)
- [16] Ross Girshick. Fast r-cnn. In *International Conference on Computer Vision (ICCV)*, 2015. [1](#)
- [17] Ross Girshick, Jeff Donahue, Trevor Darrell, and Jitendra Malik. Rich feature hierarchies for accurate object detection and semantic segmentation. In *Proceedings of the IEEE/CVF Conference on Computer Vision and Pattern Recognition (CVPR)*, 2014. [1](#)
- [18] Suyog Gupta, Ankur Agrawal, Kailash Gopalakrishnan, and Pritish Narayanan. Deep learning with limited numerical precision. In *International Conference on Machine Learning (ICML)*, pages 1737–1746, 2015. [1](#), [3](#)
- [19] Matan Haroush, Itay Hubara, Elad Hoffer, and Daniel Soudry. The knowledge within: Methods for data-free model compression. In *Proceedings of the IEEE/CVF Conference on Computer Vision and Pattern Recognition*, pages 8494–8502, 2020. [3](#), [10](#)
- [20] M. Haroush, I. Hubara, E. Hoffer, and D. Soudry. The knowledge within: Methods for data-free model compression. In *2020 IEEE/CVF Conference on Computer Vision and Pattern Recognition (CVPR)*, pages 8491–8499, 2020. [13](#)
- [21] Kaiming He, Xiangyu Zhang, Shaoqing Ren, and Jian Sun. Deep residual learning for image recognition. In *Proceedings of the IEEE/CVF Conference on Computer Vision and Pattern Recognition (CVPR)*, 2016. [2](#), [8](#), [10](#), [11](#)
- [22] K. He, X. Zhang, S. Ren, and J. Sun. Deep residual learning for image recognition. In *2016 IEEE Conference on Computer Vision and Pattern Recognition (CVPR)*, pages 770–778, 2016. [9](#)
- [23] Xiangyu He, Qinghao Hu, Peisong Wang, and Jian Cheng. Generative zero-shot network quantization, 2021. [1](#), [2](#), [3](#)
- [24] Benoit Jacob, Skirmantas Kligys, Bo Chen, Menglong Zhu, Matthew Tang, Andrew Howard, Hartwig Adam, and Dmitry Kalenichenko. Quantization and training of neural networks for efficient integer-arithmetic-only inference. In *Proceedings of the IEEE Conference on Computer Vision and Pattern Recognition*, pages 2704–2713, 2018. [1](#), [3](#), [10](#)
- [25] Krizhevsky, Alex, Sutskever, Ilya, Hinton, and E. Geoffrey. Imagenet classification with deep convolutional neural networks. *Communications of the ACM*, 2017. [1](#)
- [26] Alex Krizhevsky, Geoffrey Hinton, et al. Learning multiple layers of features from tiny images. 2009. [8](#), [9](#)
- [27] Alex Kulesza and Ben Taskar. Determinantal point processes for machine learning. *arXiv preprint arXiv:1207.6083*, 2012. [6](#)
- [28] Fuxin Li, Yunshan Fu, Yu-Hong Dai, Cristian Sminchisescu, and Jue Wang. Kernel learning by unconstrained optimization. In *Artificial Intelligence and Statistics*. PMLR, 2009. [6](#)
- [29] Rundong Li, Yan Wang, Feng Liang, Hongwei Qin, Junjie Yan, and Rui Fan. Fully quantized network for object detection. In *Proceedings of the IEEE/CVF Conference on Computer Vision and Pattern Recognition (CVPR)*, 2019. [1](#)
- [30] Yuhang Li, Ruihao Gong, Xu Tan, Yang Yang, Peng Hu, Qi Zhang, Fengwei Yu, Wei Wang, and Shi Gu. Breq: Pushing the limit of post-training quantization by block reconstruction. In *International Conference on Learning Representations*, 2021. [1](#)
- [31] Jing Liu, Bohan Zhuang, Zhuangwei Zhuang, Yong Guo, Junzhou Huang, Jinhui Zhu, and Mingkui Tan. Discrimination-aware network pruning for deep model compression. *IEEE Transactions on Pattern Analysis and Machine Intelligence*, pages 1–1, 2021. [1](#)
- [32] Yuang Liu, Wei Zhang, and Jun Wang. Zero-shot adversarial quantization. In *Proceedings of the IEEE/CVF Conference on Computer Vision and Pattern Recognition (CVPR)*, June 2021. [1](#), [2](#), [3](#), [10](#)
- [33] A. Mordvintsev, Christopher Olah, and M. Tyka. Inceptionism: Going deeper into neural networks. 2015. [11](#)
- [34] Markus Nagel, Rana Ali Amjad, Mart van Baalen, Christos Louizos, and Tijmen Blankevoort. Up or down? adaptive rounding for post-training quantization, 2020. [1](#), [3](#), [13](#)
- [35] Markus Nagel, Mart van Baalen, Tijmen Blankevoort, and Max Welling. Data-free quantization through weight equalization and bias correction. In *International Conference on Computer Vision (ICCV)*, 2019. [1](#), [3](#), [9](#), [12](#)
- [36] Augustus Odena, Christopher Olah, and Jonathon Shlens. Conditional image synthesis with auxiliary classifier gans. In *International Conference on Machine Learning (ICML)*, 2017. [8](#)
- [37] Jiangmiao Pang, Kai Chen, Jianping Shi, Huajun Feng, Wanli Ouyang, and Dahua Lin. Libra r-cnn: Towards balanced learning for object detection. In *Proceedings of the IEEE/CVF Conference on Computer Vision and Pattern Recognition (CVPR)*, 2019. [1](#)
- [38] Eunhyeok Park, Sungjoo Yoo, and Peter Vajda. Value-aware quantization for training and inference of neural networks, 2018. [10](#)
- [39] Haoteng Qin, Zhongang Cai, Mingyuan Zhang, Yifu Ding, Haiyu Zhao, Shuai Yi, Xianglong Liu, and Hao Su. Bipointnet: Binary neural network for point clouds, 2020. [1](#)
- [40] Haoteng Qin, Ruihao Gong, Xianglong Liu, Xiao Bai, Jingkuan Song, and Nicu Sebe. Binary neural networks: A survey. *Pattern Recognition*, 2020. [1](#)

- [41] Haotong Qin, Ruihao Gong, Xianglong Liu, Mingzhu Shen, Ziran Wei, Fengwei Yu, and Jingkuan Song. Forward and backward information retention for accurate binary neural networks. In *IEEE/CVF Conference on Computer Vision and Pattern Recognition (CVPR)*, June 2020. 1
- [42] Shaoqing Ren, Kaiming He, Ross Girshick, and Jian Sun. Faster r-cnn: Towards real-time object detection with region proposal networks, 2016. 1
- [43] Mark Sandler, Andrew G. Howard, Menglong Zhu, Andrey Zhmoginov, and Liang-Chieh Chen. Mobilenetv2: Inverted residuals and linear bottlenecks. In *Proceedings of the IEEE/CVF Conference on Computer Vision and Pattern Recognition (CVPR)*, 2018. 2, 8, 11
- [44] Xu Shoukai, Li Haokun, Zhuang Bohan, Liu Jing, Cao Jiezhong, Liang Chuangrun, and Tan Mingkui. Generative low-bitwidth data free quantization. In *European Conference on Computer Vision (ECCV)*, 2020. 1, 2, 3, 7, 11
- [45] Karen Simonyan and Andrew Zisserman. Very deep convolutional networks for large-scale image recognition. *arXiv preprint arXiv:1409.1556*, 2014. 1, 2, 8, 9
- [46] Wonyong Sung, Sungho Shin, and Kyuyeon Hwang. Resiliency of deep neural networks under quantization. *arXiv preprint arXiv:1511.06488*, 2015. 9
- [47] Christian Szegedy, Wei Liu, Yangqing Jia, Pierre Sermanet, Scott Reed, Dragomir Anguelov, Dumitru Erhan, Vincent Vanhoucke, and Andrew Rabinovich. Going deeper with convolutions. In *Proceedings of the IEEE/CVF Conference on Computer Vision and Pattern Recognition (CVPR)*, 2015. 1
- [48] Christian Szegedy, Vincent Vanhoucke, Sergey Ioffe, Jon Shlens, and Zbigniew Wojna. Rethinking the inception architecture for computer vision. In *Proceedings of the IEEE conference on computer vision and pattern recognition*, pages 2818–2826, 2016. 2, 8, 10, 11
- [49] Zhiqiang Tang, Xi Peng, Kang Li, and Dimitris N. Metaxas. Towards efficient u-nets: A coupled and quantized approach. *IEEE Transactions on Pattern Analysis and Machine Intelligence*, 42(8):2038–2050, 2020. 1
- [50] Frederick Tung and Greg Mori. Deep neural network compression by in-parallel pruning-quantization. *IEEE Transactions on Pattern Analysis and Machine Intelligence*, 42(3):568–579, 2020. 1
- [51] Yiru Wang, Weihao Gan, Wei Wu, and Junjie Yan. Dynamic curriculum learning for imbalanced data classification. In *International Conference on Computer Vision (ICCV)*, 2019. 1
- [52] Yiru Wang, Weihao Gan, Jie Yang, Wei Wu, and Junjie Yan. Dynamic curriculum learning for imbalanced data classification. In *International Conference on Computer Vision (ICCV)*, October 2019. 1
- [53] Ziwei Wang, Jiwen Lu, Ziyi Wu, and Jie Zhou. Learning efficient binarized object detectors with information compression. *IEEE Transactions on Pattern Analysis and Machine Intelligence*, pages 1–1, 2021. 1
- [54] Ziwei Wang, Jiwen Lu, and Jie Zhou. Learning channel-wise interactions for binary convolutional neural networks. *IEEE Transactions on Pattern Analysis and Machine Intelligence*, pages 1–1, 2020. 1, 3
- [55] Yanlu Wei, Renshuai Tao, Zhangjie Wu, Yuqing Ma, Libo Zhang, and Xianglong Liu. Occluded prohibited items detection: An x-ray security inspection benchmark and de-occlusion attention module. In *Proceedings of the 28th ACM International Conference on Multimedia*, page 138–146, 2020. 1
- [56] Yudong Wu, Yichao Wu, Ruihao Gong, Yuanhao Lv, Ken Chen, Ding Liang, Xiaolin Hu, Xianglong Liu, and Junjie Yan. Rotation consistent margin loss for efficient low-bit face recognition. In *Proceedings of the IEEE/CVF Conference on Computer Vision and Pattern Recognition (CVPR)*, June 2020. 1
- [57] Jie Yang, Jiarou Fan, Yiru Wang, Yige Wang, Weihao Gan, Lin Liu, and Wei Wu. Hierarchical feature embedding for attribute recognition. In *Proceedings of the IEEE/CVF Conference on Computer Vision and Pattern Recognition (CVPR)*, June 2020. 1
- [58] Hongxu Yin, Pavlo Molchanov, Zhizhong Li, Jose M. Alvarez, Arun Mallya, Derek Hoiem, Niraj K. Jha, and Jan Kautz. Dreaming to distill: Data-free knowledge transfer via deepinversion, 2020. 13
- [59] Xiangguo Zhang, Haotong Qin, Yifu Ding, Ruihao Gong, Qinghua Yan, Renshuai Tao, Yuhang Li, Fengwei Yu, and Xianglong Liu. Diversifying sample generation for accurate data-free quantization. In *Proceedings of the IEEE/CVF Conference on Computer Vision and Pattern Recognition (CVPR)*, June 2021. 1, 2, 3
- [60] Xiangyu Zhang, Xinyu Zhou, Mengxiao Lin, and Jian Sun. Shufflenet: An extremely efficient convolutional neural network for mobile devices. *Proceedings of the IEEE/CVF Conference on Computer Vision and Pattern Recognition (CVPR)*, 2018. 2, 8, 10, 11
- [61] Ritchie Zhao, Yuwei Hu, Jordan Dotzel, Christopher De Sa, and Zhiru Zhang. Improving neural network quantization without retraining using outlier channel splitting. *arXiv preprint arXiv:1901.09504*, 2019. 1, 3, 9
- [62] Bohan Zhuang, Chunhua Shen, Mingkui Tan, Lingqiao Liu, and Ian Reid. Structured binary neural networks for accurate image classification and semantic segmentation. In *Proceedings of the IEEE/CVF Conference on Computer Vision and Pattern Recognition (CVPR)*, 2019. 1
- [63] Bohan Zhuang, Mingkui Tan, Jing Liu, Lingqiao Liu, Ian Reid, and Chunhua Shen. Effective training of convolutional neural networks with low-bitwidth weights and activations. *IEEE Transactions on Pattern Analysis and Machine Intelligence*, pages 1–1, 2021. 1, 3